©2020. This manuscript version is made available under the CC-BY-NC-ND 4.0 license http://creativecommons.org/licenses/by-nc-nd/4.0/

Investigation of bubble behavior with phase change under the effect of noncondensable gas

Hongwei Jia [a], Xin Xiao [b], Yanming Kang [a,*]

[a] School of Environmental Science and Engineering, Donghua University, Shanghai 201620, China

[b] School of Engineering and Computer Science, University of Hull, HU6 7RX, United Kingdom

*Corresponding author. Tel.: +86-21-67792554; fax: +86-21-67792522.

E-mail address: ymkang@dhu.edu.cn (Y. M. Kang).

Abstract: An Arbitrary-Lagrangian-Eulerian based numerical method is proposed to study the phase change bubble under the effect of noncondensable gas (NCG). In order to validate the underlying mathematical model, benchmark tests, including the bubble growth in quiescent superheated liquid and the condensation of rising bubble with NCG, are conducted. The numerical results by the phase change model, in which the mass transfer rate is directly determined by interfacial heat flux, is found to agree fairly well with analytical results, and the calculation of fluid flow and heat transfer by the present numerical approach is reasonable. Moreover, the numerical results of free rising bubble condensation with NCG are found to present good agreement with the experimental data on the evolution of bubble size, and the mass balance of the NCGs is proved to be achieved by the model. Finally, the subcooled boiling with NCG on a biphilic surface is numerically investigated, and the bubble behavior and internal distribution of the NCG are studied in detail. In the presence of NCG, the bubbles can even depart from the walls that are negatively superheated. The bubble keeps the bowl-shape for a long time before necking, which is consistent with the experimental observations. The contact line is found to

stay at the boundary between the hydrophilic and hydrophobic surfaces. The results also show that the local accumulation of the NCG near the bubble surface decreases the local apparent saturation temperature and inhibits the condensation, and the growth and departure of bubbles is thus promoted. In addition, the amount of NGG in the bubble is found to determine whether the bubble in the subcooled boiling is detached or not.

Keywords: Noncondensable gas (NCG); Bubble dynamics; Mass transfer; Condensation; Subcooled boiling

1 Introduction

Phase change process like the condensation and evaporation has played an important role in a variety of high-efficiency mass and heat exchangers, including nuclear reaction tower, refrigeration, air conditioning radiators and heat pipe, yet it is also deeply affected by the appearance of noncondensable gas (NCG). Since Othmer (1929) discovered that a small amount of NCG could significantly reduce the heat transfer coefficient during condensation, researchers have been trying to further explore its thermodynamic mechanisms (Collier, 1987; Huang et al., 2015).

In the past few decades, studies on the phase change process with the NCG focused on the filmwise condensation, which has been systematically studied by numerical calculations, theoretical analysis, and experiments (Slegers and Seban, 1970; Shang, 2011). For example, Oh and Revankar (2006) presented typical experimental and theoretical studies on the film condensation with NCG, and the degradation of the condensation with NCG was investigated by introducing the steam-air mixture into a vertical tube submerged in a water pool. Additionally, an analogy for annular filmwise condensation, which was modeled based on the heat and mass transfer in boundary layer, was proposed. Revankar

and Pollock (2005) also developed a two-dimensional (2D) steady state model for convective filmwise condensation of steam-air mixture, and the deterioration of heat transfer was found to be caused by the accumulation of NCG.

There exist numerous studies on the filmwise condensation because the heat and mass transfer process can be simplified as a diffusion layer, and the heat transfer coefficient can be evaluated by a modified Nusselt solution (Hampson, 1951). In contrast, the complete simulation on bubble condensation with NCG is a rather complicated process which includes deformed phase boundaries, diffused NCG and its local accumulation, and gas dissolution in liquid, as well as the coupling interaction between them. For example, the variation of initial mole fraction of NCG (x_0), was found to cause different bubble behaviors, i.e., collapse to many microbubbles suddenly (x_0 < 2.5%), split up into several tiny bubbles (2.5% < x_0 < 7.5%), and keep infrangible (x_0 > 7.5%), which were reported in the experimental study of the bubble condensation in water with high subcooling condition (T_{sub} = 85 K) by Tang et al. (2015). Therefore, studies on bubble condensation involving NCG are still insufficient, especially by numerical methods, though many investigations have been conducted on the simple bubble condensation process in the past years. The representative numerical studies on bubble condensation are summarized in Table 1.

Table 1 Phase change models related to bubble condensation.

Literature	Interface tracking method	The phase change model
Jeon et al. (2011)	VOF	$m_f = h_i A_b \left(T_{sat} - T_l\right)/h_{fg}$, $Nu = \frac{h_i D_s}{\lambda_l} = 0.2575\,\mathrm{Re}_b^{0.7}\,\mathrm{Ja}_l^{-0.2043}\,\mathrm{Pr}_l^{-0.4564}$
Pan et al. (2012)	VOF	$m_f = h_i A_b \left(T_{sat} - T_l\right)/h_{fg}$, $Nu = 0.2575\,\mathrm{Re}_b^{0.7}\,\mathrm{Ja}_l^{-0..2043}\,\mathrm{Pr}_l^{-0.4564}$, in large channel $Nu = 0.6\,\mathrm{Re}_b^{1/2}\,\mathrm{Pr}_l^{1/3}\left(1-\mathrm{Ja}_l^{0.1}Fo_b\right)$, in narrow channel

Qu et al. (2016a, 2016b)	Euler-Euler method	$m_f = hA_b\left(T_{sat} - T_l\right)/h_{fg}$, $A_b = 6\alpha/d$ $Nu = 2.0 + 0.6\,\mathrm{Re}_b^{0.5}\,\mathrm{Pr}_l^{-0.33}$, $0 \le \mathrm{Re} < 766.06$, $0 \le \mathrm{Pr} < 250$ $Nu = 2.0 + 0.27\,\mathrm{Re}_b^{0.62}\,\mathrm{Pr}_l^{-0.33}$, $766.06 \le \mathrm{Re}$, $0 \le \mathrm{Pr} < 250$
Tian et al. (2010)	MPS	$\dot{q} = \rho_l c_{pl} \sum_{i=\text{interface}} \left[\Delta V\left(T_i^{t+\Delta t} - T_i^t\right)\right]$, $m_f = \dot{q}/h_{fg}$
Zeng et al. (2015)	CLSVOF	$j = \dfrac{T - T_{sat}}{R_{\text{int}} h_{fg}}$, $R_{\text{int}} = \dfrac{2-\chi}{\chi}\dfrac{\sqrt{2\pi R_{gas}}}{h_{fg}}\dfrac{T_{sat}^{3/2}}{\rho_v}$

Jeon et al. (2011) numerically investigated the behavior of condensing bubble by a 2D volume of fluid (VOF) method. The phase change model was obtained by the interfacial heat transfer coefficient which was estimated by an empirical formula, as shown in Table 1. Pan et al. (2012) simulated the bubble condensation in vertical rectangular channel by using a three-dimensional (3D) VOF method. They used two empirical correlations in the phase change model and distinguished the applicable range by channel size, and the simulations agree well with the experiments by Kamei and Hirarta (1990). Qu et al. (2016a, 2016b) also employed empirical correlations in the simulation of steam-air jet condensation based on an Euler-Euler method, in which the bubbles were simplified as sphere particles. However, the limitation of using the empirical correlations in phase change model (i.e., empirical phase change mode) is obvious, that is, it can only solve the problems under the corresponding working conditions. In an earlier work, Tian et al. (2010) numerically studied the single steam bubble condensation by moving particle semi-implicit (MPS) method in which the aqueous phase was modeled using moving particles and the interface was tracked by the topological position of interfacial particles. The interfacial heat flux was determined according to the energy variation of interfacial liquid layer, and, as listed in Table 1, ΔV is the interface volume of the interfacial layer corresponding with the interfacial particle size specified by the numerical convergence. Recently, Zeng et al. (2015) studied the bubble condensation based on a coupled level set and volume of fluid method (CLSVOF) by the open

source code of OpenFOAM. The phase change model, as shown in Table 1, was derived from the local superheat and the interfacial heat resistance R_{int}. In a previous paper, we used a modified model of this one by a smearing approach to maintain the numerical stabilization on simulation of pool boiling (Jia et al., 2015), and it was found that the model need the mesh with sufficient refinement. Overall, there is still lack of a universal phase change model on the bubble condensation for numerical simulations, and an efficient and accurate phase change model should be established accordingly.

For the bubble condensation with the consideration of the NCG, the works by Kalman et al. (1987, 2002) and Lerner et al. (1987) can be regarded as the representatives studies. They presented a series of experimental and analytical studies on the condensation of organic vapor bubble (R-113, pentane and hexane) in immiscible liquid (water) and miscible liquid (R-113). In the analytical model, the mass fraction of the NCG was considered to affect the temperature driving force (i.e., the difference between the saturation temperature of the condensing species and surrounding temperature) in the phase change process and determined the apparent saturation temperature. The temperature driving force was employed in a dimensionless form following the model by Isenberg and Sideman (1970). The heat transfer rate was then estimated by the empirical correlations (Lee and Barrow, 1968) which calculate the *Nu* for the front half and rear half respectively and has also been used by Kalman et al. (1987, 2002) and and Lerner et al. (1987).

Compared to the condensation process with the NCG, subcooled boiling with the NCG is much more complex due to the interaction of evaporation and condensation. Moreover, the bubble behavior of the subcooled boiling process is more complicated, with bubble nucleation, growth, detachment and thermocapillary convection. The empirical or semi-empirical phase change model for condensation mentioned above is no longer applicable for the simulation of the subcooled boiling with the NCG, and

the phase change model, which is suitable for both evaporation and condensation, is required. Consequently, only a few numerical studies have been performed on this subject. For example, Aktinol et al. (2014) studied the subcooled boiling under microgravity condition in the presence of NCGs by employing numerical simulations, and Shen et al. (2017) simulated the subcooled nucleate boiling on a biphilic surfaces (that was, with a spatially-alternating wettability pattern). Both of these two studies attempted to solve the distribution of NCG and to introduce its influence to the heat and mass transfer during the subcooled boiling, and the comparative experiments not containing NCGs were conducted by means of vacuum or long-term boiling. In the numerical model of Aktinol et al. (2014), the mass fraction field of the NCG inside the bubble was calculated based on the Level-set method, while the dilution concentration in the liquid region remained constant. Due to the presence of the NCG, the local saturation temperatures would be changed as the local partial pressure of vapor varies.

In the study of Shen et al. (2017), a diffuse-interface model was employed to derive the phase change in the gas-liquid fluid, and the NCG volume fraction was tracked by the molecules-occupied-ratio based on the Helmholtz free-energy function of binary fluid. The role of NCG was directly reflected in the molecular transport, and phase change model had a clearer physical meaning. In the study, the influence and the accumulation of the NCG in subcooled boiling were presented in detail by a scaled simulation (i.e., in extremely small space), which gave a good evidence in understanding the experimental phenomena on the early onset of nucleate boiling on the biphilic surface. These two numerical studies (Aktinol et al., 2014; Shen et al., 2017) have made great progress in providing more rigorous and appropriate models, such as accurate mass transfer models and automated two-phase fluid models. However, they still have limitations, e.g., the Aktionl's model failed to solve the accumulation of NCG at the interface while the Shen's model failed to expand to the

practical scale. Another numerical attempt on the nucleated pool boiling with NCG was carried out by Marek and Straub (2001), in which the steady-state mass transfer of a non-deformable isolated vapor bubble was simulated. The mass transfer rate was derived by the Hertz-Knudsen-Scharge equation which was consistent with the expression of interfacial heat resistance (Zeng et al., 2015; Jia et al., 2015). The influence of the accumulation of NCG and the thermocappillary convection were taken into account in their study, and it was found that the NCG inhibits the vapor condensation and induced thermocappillary flow which in turn inhibits bubble detachment.

The mechanism of the influence of the NCG is relatively clear from the above mentioned studies, i.e., the partial pressure of vapor is reduced due to the presence of the NCG and the NCG accumulation near the interface serves as a resistance for the vapor condensation. However, there is a lack of effective numerical means to simulate such process, so as to make quantitative and detailed predictions. Therefore, we aim to propose an accurate and efficient two-phase flow model with phase change in the presence of the NCG in the present study. An Arbitrary Lagrangian Eulerian (ALE) method, allowing for highly accurate hydrodynamic and interfacial mass transfer solution, is adopted as the interface tracking method here, because it has been found to be more efficient than methods of the VOF and the CLSVOF in our previous studies (Jia et al., 2015, 2019; Zhang and Jia, 2016). The phase change model based on the interfacial heat flux is developed and validated with the theoretical solution. Then, we conducted a numerical study with the modified model considering the effect of NCG on the bubble condensation process and the subcooled boiling process. The numerical results are compared with the experimental results subsequently, and the influence of the NCG on the phase change and the bubble behavior are studied in detail.

2 Mathematical model

2.1 The ALE method

As mentioned, the ALE method is used in the present study due to the good efficiency and accuracy under simple topological deformation (Falcone et al., 2018). The governing equations of the mass, momentum, energy in the ALE method for incompressible flow are written as follows, respectively:

$$\rho\nabla\cdot\mathbf{u}=0 \tag{1}$$

$$\rho\left(\frac{\partial\mathbf{u}}{\partial t}+\left(\mathbf{u}_{\mathrm{c}}\cdot\nabla\right)\mathbf{u}\right)=\nabla\cdot\left[-p\mathbf{I}+\mu\left(\nabla\mathbf{u}+\left(\nabla\mathbf{u}\right)^{T}\right)\right]+\rho\mathbf{g} \tag{2}$$

$$\rho C_{\mathrm{p}}\left(\frac{\partial T}{\partial t}+\left(\mathbf{u}_{\mathrm{c}}\cdot\nabla\right)T\right)=\nabla\cdot\left(\lambda\nabla T\right) \tag{3}$$

where ρ is the density, $\mathbf{u}$ is the velocity vector, p the pressure. Here $\mathbf{u}_{\mathrm{c}}$ denotes the convection velocity and is defined by:

$$\mathbf{u}_{\mathrm{c}}=\mathbf{u}-\mathbf{u}_{\mathrm{m}} \tag{4}$$

where $\mathbf{u}_{\mathrm{m}}$ arises from the definition of time derivatives in the coordinate system of the deformed mesh. When dealing with the two phase flow, the computational domain is decomposed into two sub-domains filled with the individual phases, and the free moving interface is tracked by moving mesh. Moreover, the mesh is deformed smoothly with given constraints, e.g. the Winslow smoothing (Jafari and Okutucu, 2016), at the moving boundaries and interfaces in the domains with free displacement.

In order to study the effect of the internal distribution of the NCG in the bubble, the concentration filed is calculated in the gas domain by a species transport equation:

$$\frac{\partial c}{\partial t}+\left(\mathbf{u}_{\mathrm{c}}\cdot\nabla\right)c=\nabla\cdot\left(D\nabla c\right) \tag{5}$$

where c is the molar concentration of the NCG, D is the diffusion coefficient. It should be noticed that a concentration flux is specified at the interface to ensure the mass conservation of NCG in the bubble, and the detail will be shown in the next section.

In the present study, the diffusion coefficients D for the binary gas systems, i.e. the air and vapor here, in the bubble are estimated by the Fuller equation (Fuller et al., 1969):

$$D_{12} = \frac{0.00143T^{1.75}}{PM_{12}^{1/2}\left[\left(\sum \upsilon\right)_1^{1/3} + \left(\sum \upsilon\right)_2^{1/3}\right]^2} \quad (6)$$

where $M_{12} = 2\left[\left(1/M_1\right) + \left(1/M_2\right)\right]^{-1}$, and M_1 and M_2 are the molecular weights of components 1 and 2, respectively. The $\sum\upsilon$ is found for each component by summing atomic diffusion volumes which are determined by the regression analysis of many experimental data, and more description could be found in Ref. (Poling et al., 2004). Take R113 bubble condensation as an example. For the R113-air mixture (i.e., 1 is R113, 2 is air), M_1 = 187.39 g/mol, M_2 = 29 g/mol, $(\sum\upsilon)_1$ =138.9 cm^3/mol and $(\sum\upsilon)_2$ =19.7 cm^3/mol.

2.2 The interfacial conditions and the phase change model

The interfacial conditions is undertaken carefully in model due to the jump of the physical properties and specific conditions between the phases. At the gas-liquid interface, the stresses are balanced by introducing a surface tension term:

$$\mathbf{n}\cdot\boldsymbol{\tau}_\mathrm{l} = \mathbf{n}\cdot\boldsymbol{\tau}_\mathrm{v} + \mathbf{f}_\mathrm{st} \quad (7)$$

where $\boldsymbol{\tau}_\mathrm{v}$ and $\boldsymbol{\tau}_\mathrm{l}$ are the total stress tensors in gas phase and liquid phase, respectively, $\mathbf{n}$ is the normal vector to the interface pointing from vapor to liquid in this study, $\mathbf{f}_\mathrm{st}$ is the surface tension force.

The evolution of the interface considering the mass transfer is determined by the interfacial velocity:

$$\mathbf{u}_\mathrm{v} = \mathbf{u}_\mathrm{l} + m_\mathrm{f}\left(\frac{1}{\rho_\mathrm{v}} - \frac{1}{\rho_\mathrm{l}}\right)\mathbf{n} \quad (8)$$

$$\mathbf{u}_\mathrm{mesh} = \left(\mathbf{u}_\mathrm{v}\cdot\mathbf{n} - \frac{m_\mathrm{f}}{\rho_\mathrm{v}}\right)\mathbf{n} \quad (9)$$

where $\mathbf{u}_\mathrm{l}$ and $\mathbf{u}_\mathrm{v}$ are the velocities of the liquid and gas phases, respectively. $\mathbf{u}_\mathrm{mesh}$ is the velocity of mesh

between the two fluids, and m_f is the mass flux across the phase interface. It should be noted that the interfacial velocity is derived from the mass conservation across the interface (i.e., from one phase to another), and more detailed information could be found in our previous study (Jia et al., 2019) or the relevant description of Jafari and Okutucu (2016).

Different from the VOF or the CLSVOF method, the interface in the ALE method has no thickness, and more importantly, the heat fluxes on each side can be solved directly. So the interfacial heat flux across the phase interface can be calculated, and the interfacial mass transfer rate can be simply evaluated from the net heat flux (Sato and Ničeno, 2013):

$$m_f = \left(q_l + q_v\right)/h_{fg} \tag{10}$$

where h_{fg} is the latent heat during the phase change (J/kg), and q_l and q_v are the heat fluxes from the liquid and vapor sides of the interface, respectively, which are defined as follows:

$$q_l = \lambda_l \left(\nabla T_l\right) \cdot \mathbf{n} \tag{11}$$

$$q_v = -\lambda_v \left(\nabla T_v\right) \cdot \mathbf{n} \tag{12}$$

where ∇T_v and ∇T_l are the temperature gradients in the vapor and liquid phase, respectively.

A schematic of the heat flux distribution is given in Fig. 1, where **n** is the normal direction of the interface (outward from the domain of the vapor phase). It can be seen that q_v is the heat flux from the vapor phase to the interface while the direction of q_l is opposite. The present mass transfer model can not only avoid the artificial setting of uncertain parameters (e.g., χ, h_e, h_c), but also avoid the limitation of applicable conditions of the semi-empirical or empirical phase change model.

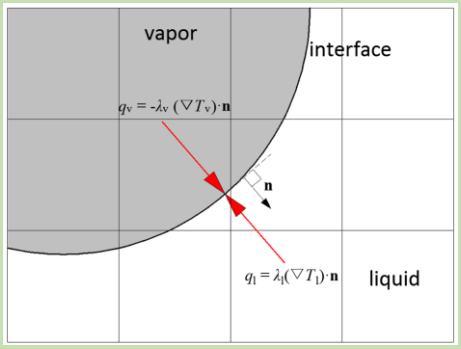

Fig. 1 The heat flux at the interface.

It should be noted that the volume migration due to the interface deformation will cause the quality of the NCG to be unconserved during the calculation. However, the amount of the NCG is almost unchanged as no addition or reduction happens during the phase change process in real application. Meanwhile, the NCG will accumulate as the vapor component decreases during the condensation process, and will be diluted as the steam increases with the evaporation.

In order to describe this phenomenon and to ensure the mass conservation of the NCG in the bubble, a concentration flux is added at the gas-liquid interface, and the value is determined by an additional test function, which is:

$$test\left(\Phi_{f,t}\right)\left(\oint_{\Omega,0} c_{g,ini} d\nu - \oint_{\Omega,t} c_{g,t} d\nu\right) = 0 \tag{13}$$

Where $\oint_{\Omega,t} c_{g,t} d\nu$ is molar amount of the NCG in the bubble, and $\oint_{\Omega,0} c_{g,ini} d\nu$ is the initial amount of the NCG. The test function is solved by the weak form and the numerical approach is similar to the re-initialization process in the Level-set method. Finally, the concentration flux at the interface is written as:

$$\Phi_{\text{int}} = \Phi_{\text{f,t}} - c_{\text{g,t}} \mathbf{u} \cdot \mathbf{n}$$

where the second term on the right side of the equation is the net flux caused by the moving mesh which also cannot be disregarded. Based on the above numerical process, the mass conservation of the

NCG is achieved when solving the concentration distribution in bubble.

The numerical study is conducted based the commercial software package COMSOL Multiphysics, and the conservation equations (momentum, continuity, energy and species) are discretized through the Galerkin method. Here, a streamline diffusion method is necessary to stabilize the solution, because the convection is significant in the present study. The mass transfer model and the conservative correction approach for the NCG as well an accelerating reference systems, which is used to synchronize the computational domain with the free rising bubble motion, are implemented by solving the user defined weak form equations. In order to resolve the problem for the mesh deformation, an automatic re-meshing technique is adopted, in which the computational domain is re-meshed when the mesh distortion becomes larger than a given limit (e.g., 2.0 in the study). The maximum time step is chosen automatically depending on the requirement of stability, and the tolerance is set to 0.001 for all the variables (u, p, c, etc.) to control the relative error in each time step.

3 Results and discussion

In this section, the numerical method in the study is first verified with a benchmark test, i.e., simulations for single bubble growth in superheated liquid. The numerical results are compared with the theoretical solutions, and the calculations of the phase change and fluid mechanics are proved to be reliable. Subsequently, the condensation of a free rising bubble in subcooled liquid and the process of subcooled pool boiling are studied considering the presence of the NCG. The results are compared with the experimental data from literatures, and the detail of the influence of the NCG on heat and mass transfer will be discussed.

3.1 The bubble growth in quiescent superheated liquid

The simulation of a single bubble growth in superheated liquid has always been used as benchmark test to verify numerical model on the solution of the phase change and hydrodynamic performance (Kunkelmann and Stephan, 2009). The analysis of Plesset and Zwick (1954) suggested that the growth of a single bubble could be divided into two stages: the inertia controlled stage and asymptotic stage. The former is attributed to the momentum interaction between the gas and surrounding liquid, and the latter is determined by the heat transfer. In addition, Scriven (1959) presented a theoretical analysis of bubble growth at the asymptotic stage when ignoring viscous and surface tension effects, and the bubble radius could be evaluated as a function of time:

$$R(t) = 2\beta\sqrt{at} \tag{14}$$

where a is liquid thermal diffusivity and β is a growth constant obtained from (Sato and Ničeno, 2013):

$$\frac{\rho_{\mathrm{l}} c_{\mathrm{pl}} T_{\mathrm{sup}}}{\rho_{\mathrm{v}}\left(h_{fg} + \left(c_{\mathrm{pl}} - c_{\mathrm{pv}}\right)T_{\mathrm{sup}}\right)} = 2\beta^2 \int_0^1 \exp\left(-\beta^2\left(\left(1-\zeta\right)^{-2} - 2\left(1-\frac{\rho_{\mathrm{v}}}{\rho_{\mathrm{l}}}\right)\zeta - 1\right)\right) d\zeta \tag{15}$$

where T_{sup} is the superheat of liquid, i.e., T_{∞}-T_{sat}.

The numerical tests are carried out in cases with working fluids of water, R134a and HFE-7100 which allow the availability in various properties. The thermophysical properties for these working fluids in the liquid phase and vapor phase at respective saturation conditions are listed in Table 2. Moreover, the parameters are in accordance with the numerical studies of Magnini (2012) in which a complete phase change boiling model by the VOF method was presented and verified by the same benchmark test. In order to reduce the computational costs, an axisymmetric coordinate system is used, and a single circle bubble with the radius of 0.1 mm is placed at the origin point of the computation domain initially.

Table 2 Thermophysical properties used in the numerical tests.

Test fluid	Phase	ρ (kg/m^3)	c_p (J/(kg K)	λ (W/m K)	ν (m^2/s)	σ (N/m)	M (g/mol)	h_{fg} (kJ/kg)
R134a	Liquid	1388	1270	0.106	4.0×10^{-4}	0.016	102	219.5
(0.84bar, 243K)	Vapor	4.43	720	0.009	9.64×10^{-6}			
Water	Liquid	958	4220	0.679	2.77×10^{-4}	0.059	18	2257
(1 bar, 373 K)	Vapor	0.597	2030	0.025	1.25×10^{-5}			
HFE-7100	Liquid	1425	1430	0.0618	3.56×10^{-4}	0.0136	250	117.8
(0.52bar, 314K)	Vapor	5.15	900	0.00103	1.11×10^{-5}			

According to the Eq. (15), the growth constant β can be calculated when the superheat T_{sup} is given, and as a function of the superheat, the variation of β with T_{sup} is plotted in Fig. 2.

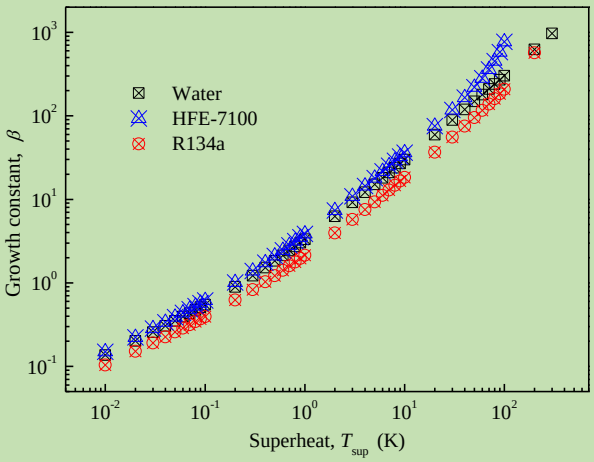

Fig. 2 The growth constants for the working fluids in the numerical tests.

It can be seen from Fig.2 that the growth constant increase gradually with the superheat, and there are slight differences in the values between different working fluids. Taking the case with T_{sup} = 5 K as an example, the growth constants are 15.10, 18.02 and 9.33 for the water, HFE-7100 and R134a, respectively. When the growth constants are known, the growths of the bubble size for these three fluids can be obtained directly by Eq. (14).

Fig. 3 gives the comparison between the numerical and analytical results of the change of the bubble size, and it can be seen that the numerical results agree well with the analytical solutions.

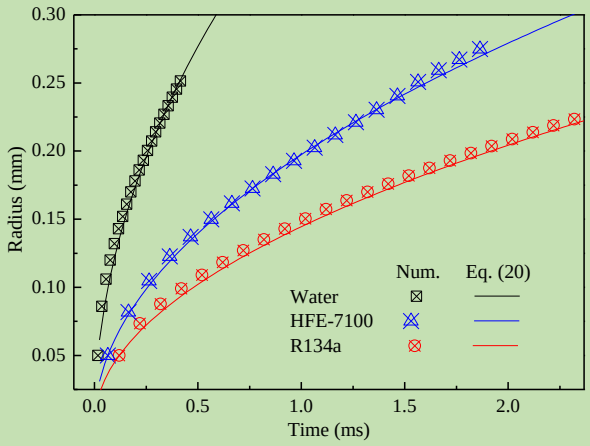

Fig. 3 Numerical and analytical results of the bubble radius over time (T_{sup} = 5 K).

From Fig. 3, it can also be found that the start times of the numerical and analytical results are adjusted with the bubble radius of 0.05 mm to ensure that these two results can correspond with each other. The water bubble grows much quickly than others even if its growth constant is not the largest, because the overall growth behavior is related to both the growth constant and thermal diffusion coefficient. In addition, the numerical procedure is found to be a good computational way that all the calculations can be completed in half an hour by a small workstation (Intel Xeon(R) CPU E5-2630v, 2.40 GHz, 32G RAM), compared to more than 2 hours using our previous VOF method (Jia et al., 2015). Moreover, in the present calculation, it is not necessary to arrange a thin thermal boundary layer around the interface on the liquid side at the initial moment to avoid calculation of divergence like Magnini (2012).

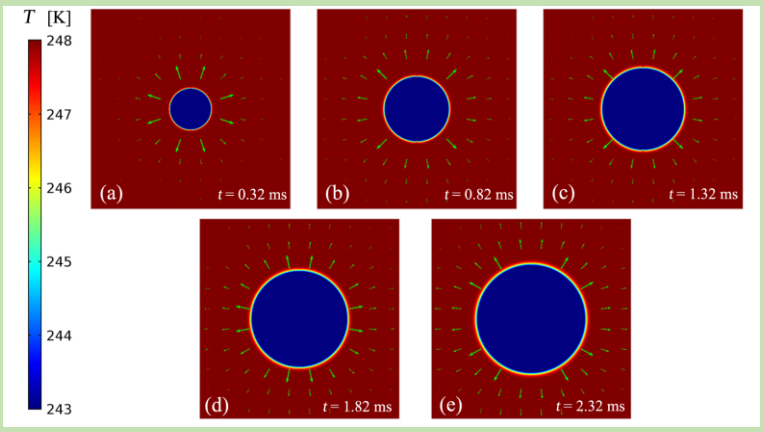

Fig. 4 Distributions of temperature and velocity vector for R134a (T_{sup} = 5 K).

Fig. 4 shows the instantaneous bubble shapes and the corresponding distributions of the temperature and velocity vector for R134a. It can be seen that the bubble maintains a regular spherical shape during the bubble growth in the statics liquid with constant superheat under the gravity-free condition. Meanwhile, the velocity vectors regularly point to the liquid side without any 'spurious' convection during the bubble growth. These both indicate that the present model is able to accurately solve the temperature and velocity field of a two-phase flow with phase change and interface deformation.

Furthermore, the calculated temperature inside the bubble maintains at the saturation temperature without any constraints, which indicate that the present model can accurately obtain the temperature distribution of each phase without any artificial settings.

Fig. 5 depicts the heat fluxes on the liquid and vapor sides used in the phase change model to calculate the interfacial mass transfer rate. It can be seen that the heat fluxes keep almost constant along the bubble surface, which is consistent with the conditions of spherical bubbles in an infinite quiescent domain and proves the accuracy of the present model. Meanwhile, the value of $|q_l|$ is about 4.4×10^4 W/m^2 while the $|q_v|$ is 1.2×10^{-2} W/m^2, and the former one is about six orders of magnitude larger than the latter. It can be found that the interfacial heat transfer is dominated by the heat transfer in the liquid phase whereas the heat transfer in the vapor phase can be almost ignored for simplification, which has been widely considered in the previous numerical studies of evaporation (Esmaeeli and Tryggvason, 2004). However, when there is condensation, the heat transfer in the vapor phase become important too, so the heat fluxes on the both sides are taken into account during the calculation of the mass transfer.

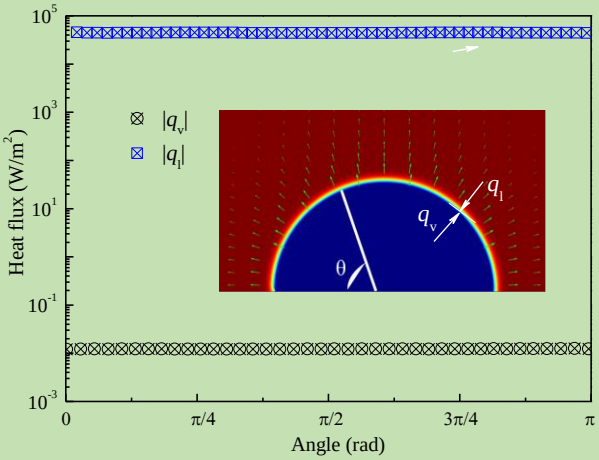

Fig. 5 The heat fluxes on the liquid and vapor sides of the interface (R134a, t = 2 ms).

3.2 The rising bubble condensation with the NCG

Although some numerical studies on the condensation have discussed the bubble shrinkage, most of them failed to consider the effects of the NCGs, which could lead to inaccuracies because the bubble collapse would significantly slow down due to the appearance of the NCG. The simulations presented in this section involve condensation at the bubble surface as well as the effect of the NCG, and thus the validation becomes considerably more challenging. In the present study, the experimental study of Kalman (2003) with careful selection is chosen to verify the numerical results, in which the visualizations of a single R113 bubble condensation were revealed and the bubble collapses were observed carefully. More importantly, the NCG was taken into account and measured quantitatively in the experiments, which could be a very good reference for comparison with the numerical results.

In the presence of the NCG, the apparent saturation temperature of the vapor would be reduced due to lower partial pressure according to the Dalton Law, and the total pressure equals the summation of the partial pressures:

$$P = P_v + P_g \tag{16}$$

where P is the total pressure, and P_v and P_g are the partial pressure of the vapor component and the

NCG, respectably. Subsequently, the corresponding saturation temperature of the vapor phase is estimated by the Antoine equation which is a class of semi-empirical correlation describing the relation between vapor pressure and temperature. It is derived from the Clausius-Clapeyron relation and has been widely used to estimate the vapor pressure over limited temperature ranges (Antoine, 1888). The proposed formula is shown below:

$$\log P_{\mathrm{v}} = A - \frac{B}{\left(T_{\mathrm{sat,v}} + C\right)} \tag{17}$$

where P_{v} is the partial pressure of vapor with the unit of mmHg, $T_{\mathrm{sat,v}}$ is the vapor saturation temperature and the constant values of A, B and C are related to the specified working fluid. For instance, the A, B and C of R113 are 6.88, 1099.9 and 227.5 (Sanjari et al., 2013), respectively. Base on the above equations, the saturation temperature of the vapor in appearance of NCG (i.e., $T_{\mathrm{sat,nc}}$) can be estimated, and the variation of the saturation temperature caused by the NCG could be calculated:

$$T_{sat} - T_{sat,nc} = B\frac{-\log\left(1-\Gamma\right)}{\left(A-\log P_{\infty}\right)\left[A-\log P_{\infty}-\log\left(1-\Gamma\right)\right]} \tag{18}$$

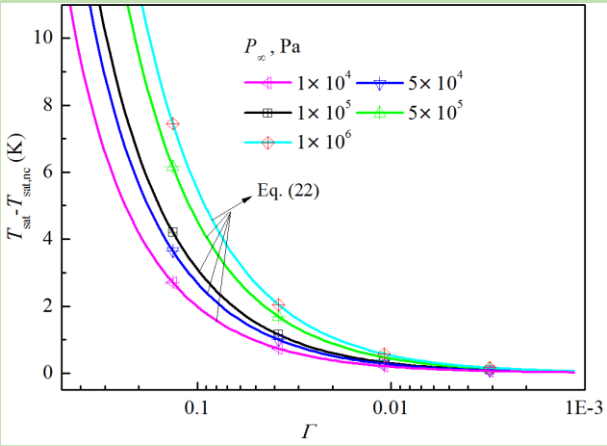

Fig. 6 Temperature deviation (T_{sat}-$T_{\mathrm{sat,nc}}$) as function of the mole fraction of NCG (Γ).

The difference of saturation temperatures between the cases with and without NCG (i.e., T_{sat}-$T_{\mathrm{sat,nc}}$) are shown in Fig. 6 as a function of the mole fraction (i.e., $\Gamma = n_{\mathrm{g}}/(n_{\mathrm{g}}+n_{\mathrm{l}})$). It can be found that the vapor saturation temperature is reduced by the NCG for all the cases and temperature deviation increases with

the mole fraction gradually and reaches 10 K after the Γ is up to 0.5. Additionally, it can be seen that the temperature deviation increases with the total pressure at the same mole fraction.

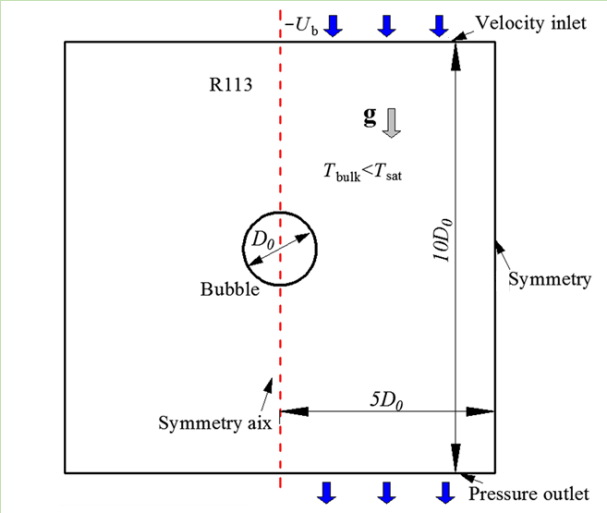

Fig. 7 The computational domain for the condensation of R113 rising bubble.

Based on the above numerical process, the influence of the NCG can be taken into account. In order to verify the entire model, the condensation process of a single rising bubble with the NCG is numerically studied. As shown in the Fig. 7, an axisymmetric computational domain is assumed, and a sphere bubble is set at the center initially. The length and width of the computational domain are set to $5D_0$ and $10D_0$, receptively. In order to save the computational resource, an accelerating coordinate system is used, in which a velocity inlet with the value of bubble rising velocity U_b is specified at the top boundary, and thus the bubble could be kept at the center. The detailed description for the method of the accelerating coordinate system could be found in our previous study (Jia et al., 2019) in which the bubble rising velocity is calculated by additional differential equations, and the proposed method is proved to be feasible and correct. In order to analyze the influence of the NCG distribution on the condensation, we calculate the condensation process of the NCG-vapor mixture with non-uniform distribution (NUD) and uniform distribution (i.e., UD, fully mixed), respectively. Here, the former calculates the transport and distribution of NCGs in bubbles, while the latter considers that the NCGs

and vapors are fully mixed in bubbles.

Fig. 8 shows the evolutions of the bubble size and the molar amount of NCG during the R113 bubble condensation. The numerical results are compared with data from the experiments of No. CFF 2122 and CFF 2221 (Kalman, 2003).

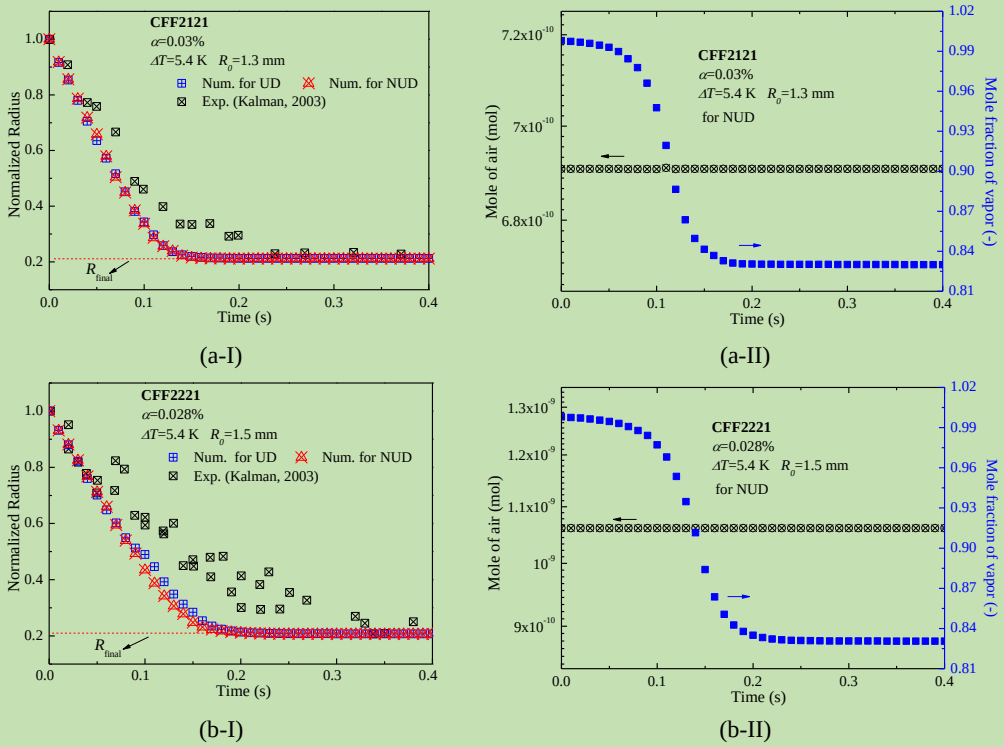

Fig. 8 Condensation of R113 bubbles in subcooled R113. (I) evolution of the bubble size. (II) evolutions of the molar amount of the NCG and the corresponding mole fraction.

It can be found that the numerical results accord with the experiment data fairly on the bubble size evolution, as shown in Figs. 8 (a-I) and (b-I). The bubble normalized radius decreases gradually until reaching the final size R_{final} which also agrees with the observation. When the initial amount of the NCG is specified, the fraction of the NCG increases as the condensation process proceeds. Subsequently, the vapor partial pressure decreases, and so dose the apparent saturation temperature T_{sat}^{*}. Meanwhile, the corresponding temperature driving force (T_{sat}^{*}-T_{∞}) falls down. The condensation is about to stop when the T_{sat}^{*} approaches the T_{∞}, and the bubble size no longer changes. As shown in the figures, the numerical results present tiny difference regardless of whether the concentration filed of the

NCG (c_g) is solved, i.e, the deviation between the results of the NUD and UD is very small. It proves that the well mixed assumption for constituent gases (Kalman and Ullmann, 1999; Ullmann and Letan 1989) in the bubble during the condensation process is available. However, this assumption is limited to the case when the bulk fluid is uniform, and the distribution of the NCG cannot be ignored when the external subcooled fluid is unevenly distributed, such as the subcooled boiling. In addition, it should be noted that there are some deviations between the experimental and simulation results, that is, the predicted bubble shrinkage rate is slightly faster than the experimental values. The reason may be the existence of Knudsen layer (Gusarov and Smurov, 2002) which is a collision-free zone adjacent to the interface and causes strong nonequilibrium. However, the existing model for Knudsen layer is often one-dimensional and depends on uncertain evaporation or condensation coefficients, ranging from 0.001 to 1 by three orders of magnitude (Zheng et al., 2018; Marek and Straub, 2001), so the Knudsen layer model is not used in the present study. But a better model is worth to be further investigated.

The changes in the mole fraction of the NCG over time are also shown in the Figs. 8 (a-II) and (b-II). It can be clearly found that the amount of NCG in the bubble is almost constant, as the derivation is less than 1×10^{-13} mol which is so small to introduce non-negligible errors on the calculation of the mass transfer. Moreover, the molar fraction of the vapor phase gradually increases as the bubble shrinks during the condensation, which cause a decrease in the interfacial saturation temperature. Then, the bubble size no longer decreases when the interfacial saturation temperature descends to the bulk fluid temperature.

Fig 9 shows the distributions of the temperature, velocity, and NCG concentration. The right side of each figure shows the temperature field and velocity vector (shown by the green arrow), while the left side shows the NCG concentration and the streamline (shown by the cyan line). The relative velocity is

the vector difference of calculated velocity and bubble velocity, $\mathbf{u} - \mathbf{u}_b$.

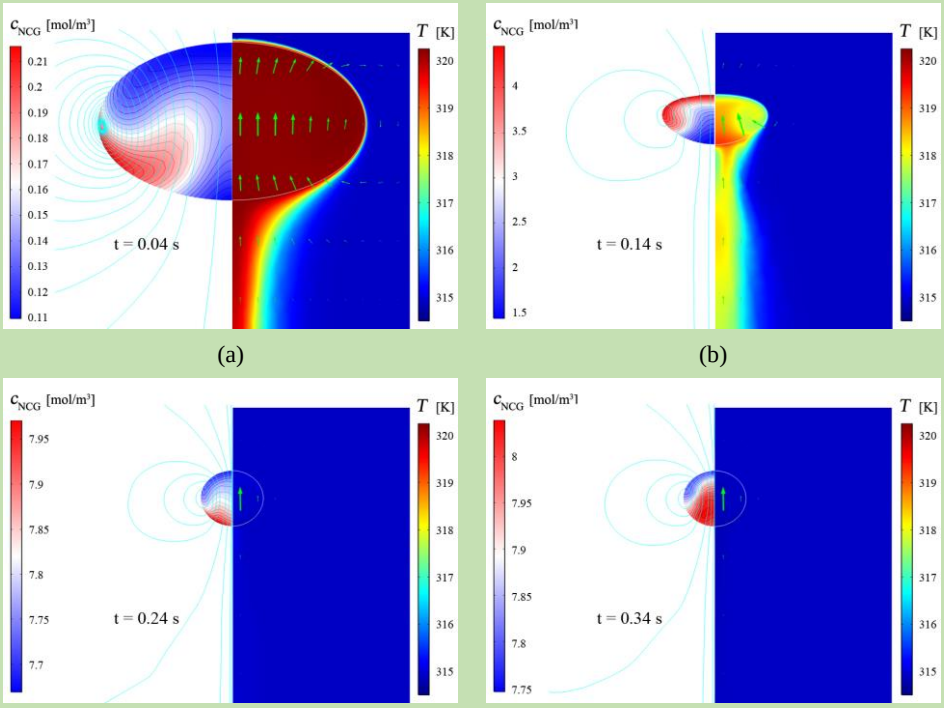

Fig. 9 Distributions of the NCG concentration (shown in the left), velocity vector and temperature (shown in the right) for the case of CFF2221. (a) t = 0.04 s, (b) t = 0.14 s, (c) t = 0.24 s, (d) t = 0.34 s.

It can be found in Fig. 9 (a-d) that the bubble size decreases during its ascending process and the shape changes from an ellipsoid to a circle. This phenomenon is reasonable according to the Grace map (Grace, 1973) which identifies bubble shapes for different *Re* numbers and bubble sizes. As shown in the figure, the temperature in the bubble decreases significantly with the bubble shrinkage until the bubble stops shrinking while the internal temperature is consistent with the temperature of the external liquid flow (T_∞). It is interesting that the accumulation of the NCG near the bubble interface during the bubble condensation is presented in the numerical results (e.g. t = 0.14 s). Combined with the temperature field diagram, it can also be seen that condensation mainly occurs at the front cap of the bubble due to the thin boundary layer, and the vapor in this area significantly reduced, and consequently, the concentration of the NCG increases to form an accumulation. In order to study the effects caused by this accumulation, the data of interfacial temperature are extracted and depicted in

Fig. 10.

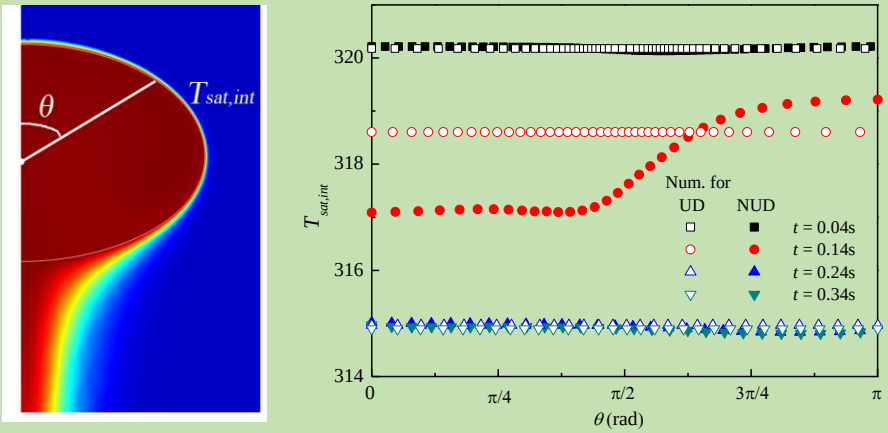

(a) (b)

Fig. 10 The interfacial temperature for the case of CFF2221.

Fig. 10 shows the temperature profile at the phase interface versus the cap angle, and the schematic of the cap angle and the interfacial temperature are depicted in the Fig. 10 (a). It can be seen that the interfacial temperature is slightly different between the cases with and without the consideration of distribution of the NCG (i.e., air) in the bubble. The interfacial temperature for the case of UD is almost constant while the temperature profile for the NUD cases change along the bubble surface especially during the shrinkage stage (e.g., t = 0.14 s). At this time, the temperature at the front cap ($\theta < \pi/2$) is smaller than that of the weak region ($\theta < \pi/2$) where the air is accumulated at the interface due to condensation which reduces the vapor partial pressure and the apparent saturation temperature. Despite the difference of the local interfacial temperature, the bubble shrinkage rates present small derivation between the two cases, shown above in the Fig. 8.

From the quantitative comparisons shown in this section, it can be concluded that the present numerical modeling is able to correctly describe the heat and mass transfer of bubble condensation with the NCG, and the numerical approach gives us an opportunity to further understand the process of subcooled boiling with the NCG in depth because the method has been verified by the numerical tests

and experimental results, and the phase change process and the influence of the NCG are found to be simulated reasonably.

3.3 The Subcooled pool boiling with NCG on a biphilic surface

The subcooled boiling with NCG is indeed a great challenge, and few studies have been reported. Because the process is really complex and it is difficult to quantitatively understand the impact of various factors including the NCG, the competition between the evaporation and the condensation, the micro-layer evaporation, the surface characteristics, etc. In order to extend the current knowledge on the subcooled boiling with NCG, a further numerical attempt on subcooled boiling with NCG is carried out in this section. The experimental results of water pool boiling presented by Shen et al. (2017) are used for the validation, and the parameters and conditions reported are adopted in the present simulation. In the experiments of Shen et al. (2017), it was found that the bubbles would remain in a bowl-like shape for a long time (tens of seconds to several hundred seconds) before the pinch-off in the subcooled boiling with the NCG. Thus, the temperature distribution inside the bubble could be measured by a microprobe, and the apparent saturation temperature was derived. Whilst the gas amount could be estimated by the Dalton's law. Therefore, the initial NCG amount of bubble in the present numerical study is estimated by the empirical formula reported by Shen et al. (2017).

In the experiments, the heated wall was a superhydrophilic TiO_2 surface coated with a hydrophobic spot with a radius of 3 mm (R_0 = 3 mm) at the center which was so called biphilic surface. Since the bubble nucleation mainly occurred at the center and bubbles kept axisymmetric in the experiments (Shen et al., 2017), we use an axisymmetric computational domain with the width and height of $5R_0$ and $10R_0$ in the present simulation, as shown in Fig. 11.

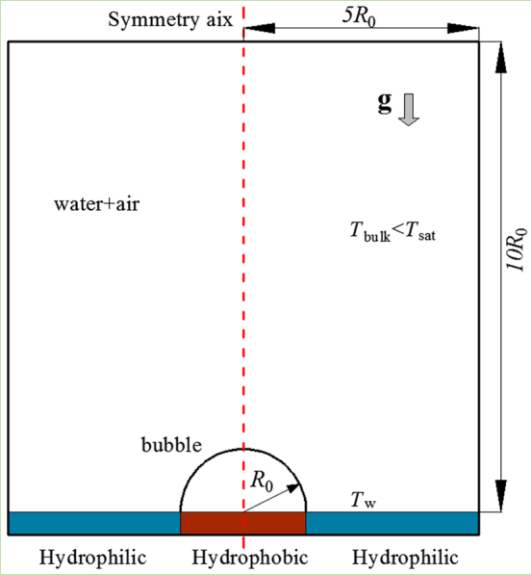

Fig. 11 The computational domain in the simulation of the subcooled boiling with NCG.

In order to make the surface essentially biphilic in the calculation, a non-uniform contact angle θ_c is assumed for the bottom wall ($\theta_c = 0.75\pi$ for $r < 3.0$ mm; $\theta_c = 0.25\pi$ for $r > 3.0$ mm) with the discontinuity at $r = 3.0$ mm replaced by a smooth transition described by a hyperbolic tangent function. The bottom wall is a fixed temperature boundary (i.e., a Dirichlet boundary) with T_w, while the right wall and top walls are insulated (i.e., Neumann boundaries). Except at the left boundary where symmetric boundary condition is applied, all bounding walls are assumed to be no-slip. As with the above simulations, the dilute presence of the NCG is only calculated in the gas phase.

The process of the bubble necking and eventual pinch-off from the surface are captured by high-speed photography, and the experimental visualization results are compared with our numerical results as shown in Fig. 12, in which all the figures are scaled by a uniform ruler and the time sequence is set to 0 at the moment of bubble pinch-off. The temperature of the bottom heated wall is set at 372.05 K (i.e., 98.9 ℃), and the degree of the subcooling of the water is 20 K. As mentioned, the initial NCG amount is estimated by empirical formulas and is set to 30.2 mol/m^3.

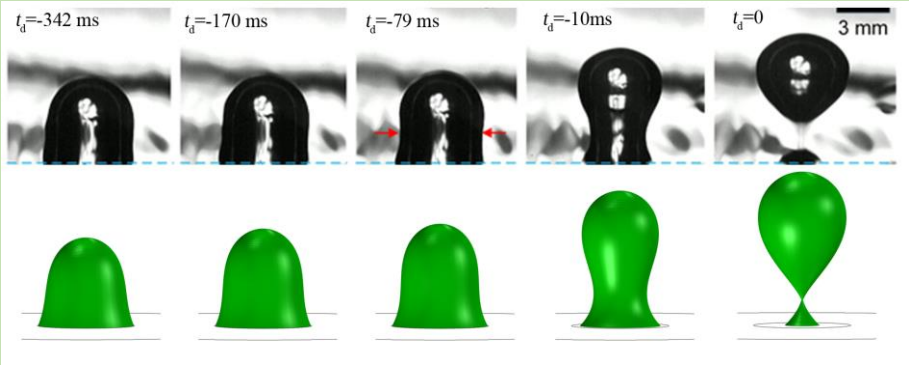

Fig. 12 Simulated bubble behaviors with the NCG presence in comparison with the experimental observations at Tw = 372.05 K.

It can be seen that the calculated bubble size and shape are consistent with the experimental results, and the bubble departure occurs after a relatively long period with the competition between the evaporation and the condensation, as shown in the figure. Moreover, the bubble is able to pinch-off while the heated wall is negatively superheated (i.e., the wall temperature being below the saturation temperature at the system pressure) because of the NCG in the bubble which decreases the apparent saturation temperature of the vapor. Furthermore, it can be found that the formation of the buckle-type bubble is derived from the circular hydrophobic point, and gas-liquid contact lines tend to stabilize at the contact boundaries between the hydrophobic and hydrophilic regions.

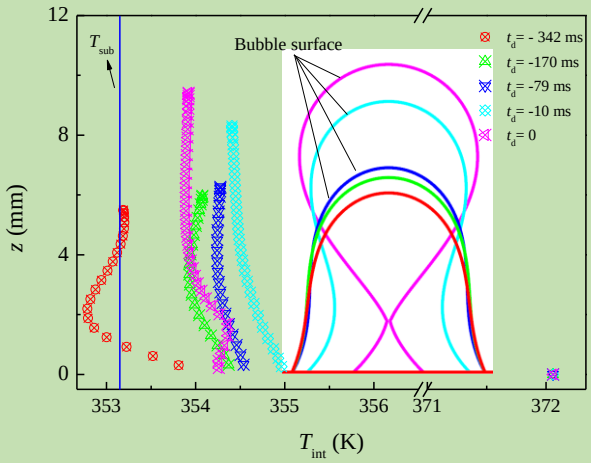

Fig. 13 The interfacial temperature of the bubble surface.

The temperature profile at the bubble surface is depicted in Fig. 13, and the different colors

correspond to the different moments from t_d = -342 ms to t_d = 0 ms. The temperatures are shown by scatters and the instantaneous bubble shapes are depicted by contour lines. The interfacial temperature is found to be much lower than the saturation temperature at the corresponding system pressure and close to the temperature of the bulk fluid T_∞. Moreover, the temperature is non-uniform along the surface from the bottom to the top because of the variation of the local concentration of the NCGs. It is interesting that the temperature at the top is slightly lower than the bottom one, which inhibits the upper condensation and narrows the disparity between the condensation and the evaporation. In addition, the temperatures at the contact lines reaches the value of T_w which is consistent with the Dirichlet boundary condition with fixed temperature.

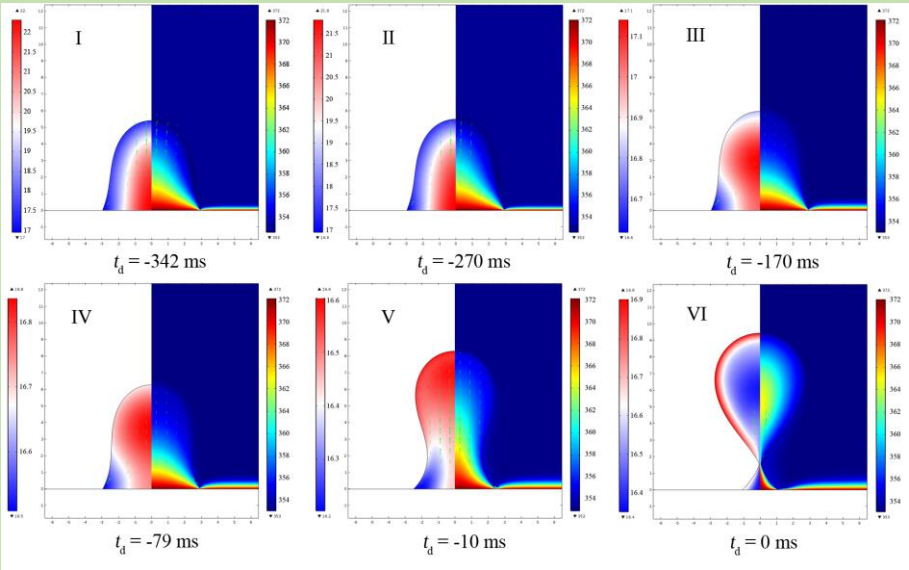

Fig. 14 The distribution of the NCG and the temperature. T_w = 372.05 K

Fig. 14 shows the distribution of the NCG concentration and the temperature fields at different times during the bubble growth and departure processes. Here, the legend for the concentration needs special attention, and it can be seen that the value range is reduced from the initial 17~22 (mol/m^3) to the 16.4~16.9 (mol/m^3) at the pinch-off, which indicates that the distribution of the NCG gradually becomes uniform.

Before the necking (I-IV), the bubble grows gradually as the evaporation dominates, and water vapor is generated at the interface. Meanwhile, the vapor saturation temperature increases due to a decrease in the concentration of the NCG at the interface. Then, the condensation begins to dominate, and the NCGs start to accumulate in the upper part of the bubble (in the red-shaded area) after the necking (IV-VI). This phenomenon is consistent with the simulation of the gas concentration distribution in the nano-bubble growth and detachment made by Shen et al. (2017). It can be found that the concentration distribution of NCG can no longer be ignored because the temperature difference between the upper and near wall fluids is large, and the local concentration of NCG directly determines whether it is evaporation or condensation.

Fig. 15 shows the evolutions of the size and final shapes of bubbles with different initial NCG concentrations. The temperatures of the heated-wall are the same and also set to 372.05 K, and the bulk water are specified with a subcooling level of 20 K.

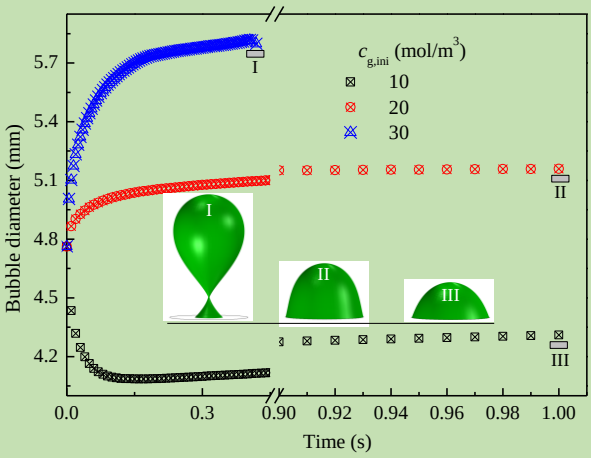

Fig. 15 The influence of the NCG on the bubble behavior.

It can be seen that the bubbles will increase or decrease significantly at the beginning and then grow at a gentle rate. Such behaviour is determined the relative concentration of the NCG which changes with the competitive mechanism (i.e., the concentration decreases when the evaporation dominates, but

increases when the condensation dominates). Take the case of $c_{g,ini}$ = 20 for example, the bubble grows quickly at initial stage, and at the same time, the relative concentration of NCG decreases, which cause increase of the interfacial vapor partial pressure. Meanwhile, the saturation temperature rises, and the evaporation is deteriorated. In short, the amount of NCG determines who has the advantage in the competition between the evaporation and the condensation, thus deciding whether bubbles grow or shrink. As shown in the insects of Fig. 15, the bubble detachment is mainly determined by the amount of NCG, and relatively stable cap bubbles can be formed on the heating surface with an appropriate amount of NCG. This phenomenon is also consistent with the observation of a long-term stable buckle-type bubble observed in experiments (Shen et al., 2017).

4 Conclusions

A numerical approach on multiphase-multicomponent transfer is developed based the ALE method in the present study. The effect of the NCG in the phase change is taken into account, and the mass conservation of the NCG is strictly enforced during the calculation. In the study, we first conduct a series of benchmark tests, including the simulations of bubble growth in superheated liquid and of the condensation of bubbles containing NCG in subcooled fluids, which show reasonable predictions. Then, the subcooled boiling with NCG is studied numerically. The main conclusions of the present study are summarized as follows:

(1) The numerical results of the bubble growth in the superheated fluid show that the predicted bubble growth agrees well with the theoretical solution, and there is no ‘spurious’ convection in the calculated flow field. The proposed model has good stability and accuracy on solving the two-phase flow with phase change.

(2) The bubble shrinkage during condensation with the NCG predicted by the present method is consistent with the experimental data. The bubble reach final size at the end of the condensation, when the interfacial saturation temperature approaches the value of the external fluid. The NCG accumulates locally during the bubble condensation, but its effect on bubble shrinkage is not obvious compared with results by uniform distribution.

(3) In the subcooled boiling, the amount of NCG determines the bubble detachment, and the bubbles can even depart from the walls that are negatively superheated in the presence of NCG. The numerical results obtain a bowl-shaped bubble on the biphilic surface, and the three phase contact line is stabilized at the hydrophobic-hydrophilic boundary. Additionally, the local accumulation of NCG causes the condensation temperature at the upper portion of the bubble to be lower than the one at the lower portion, and also contributes to deterioration of condensation and promotes the bubble detachment.

Acknowledgement

This work was supported by the Shanghai Sailing Program [Grant No. 18YF1400700]; the China Postdoctoral Science Foundation [Grant No. 2018M641891]; the National Natural Science Foundation of China [Grant No. 51578121]; the Fundamental Research Funds for the Central Universities of China [Grant No. 2232018D3-37]. The authors are very grateful to Dr. B. Shen for providing selfless detailed experimental data for the comparison and analysis.

Nomenclature

a	thermal diffusivity, m^2/s
CFF	condensation of R-113 in subcooled R-113
c	molar concentration of species, mol/m^3
c_p	specific heat, J/(kg K)

D	diffusion coefficient, m^2/s
Fo	Fourier number
g	gravity acceleration, m/s^2
h_{fg}	the latent heat (J/kg)
H	the Henry coefficient, kPa
Ja	Jakob number
m_f	mass transfer rate, kg/m^2s
M	the molecular weight, g/mol
n	molar amount, mol
Nu	Nusselt number
NUD	non-uniform distribution
p	pressure, Pa
P	partial pressure, Pa
Pr	Prandtl number
q	heat flux at the phase boundary, W/m^2
R	radius, m
Re	Reynolds number
t	time, s
T	temperature, K
ΔT	temperature difference, K
$\mathbf{u}$	velocity vector, m/s
UD	uniform distribution
V	volume, m^3
x	molar fraction, -
Greek Symbols	
α	the volume fraction, -
β	growth constant
Γ	the mole fraction, -
θ	angle, rad
λ	Thermal conductivity, W/m K
μ	dynamic viscosity, Pa·s
ν	kinematic viscosity, m^2/s
ρ	density, kg/m^3
σ	surface tension coefficient, N/m
Ω	the bubble domain
Subscripts	
0	the initial time
b	bubble
d	departure
eq	equivalent
exp	experimental
g	gas
ini	initial
int	interface

l	liquid
local	local
num	numerical
sat	saturation
sub	subcooled
sup	superheat
v	vapor
w	wall
∞, bulk	bulk flow

References

Aktinol, E., Warrier, G.R., Dhir, V.K., 2014. Single bubble dynamics under microgravity conditions in the presence of dissolved gas in the liquid. Int. J. Heat Mass Tran. 79, 251-268.

Antoine, C., 1988. Tension des vapeurs: Nouvelle relation entre les tension et les temperatures. Comptes Rendus 107, 681-836.

Collier, J.G., 1981. Convective boiling and condensation. second ed. McGraw-Hill, New York.

Esmaeeli, A., Tryggvason, G., 2004. Compuations of film boiling. Part I: numerical method. Int. J. Heat Mass Tran. 47, 5451-5461.

Falcone, M., Bothe. D., Marschall, H., 2018. D direct numerical simulations of reactive mass transfer from deformable single bubbles: An analysis of mass transfer coefficients and reaction selectivities. Chem. Eng. Sci. 177, 523-536.

Fuller, E.N., Ensley, K., Giddings, J.C., 1969. Diffusion of halogenated hydrocarbons in helium. The effect of structure on collision cross sections. J. Phys. Chem. 73, 3679-3685.

Grace, J.R., 1973. Shapes and velocities of bubbles rising in infinite liquids. Trans. Inst. Chem. Eng. 51, 116-120.

Gusarov, A.V., Smurov, I., 2002. Gas-dynamic boundary conditions of evaporation and condensation: Numerical analysis of the Knudsen layer. Phys. Fluids 14(12), 4242-4255.

Hampson, H., 1951. The condensation of steam on a metal surface. Institute of Mechanical Engineers, London, pp. 58-61.

Huang, J., Zhang, J., Wang, L., 2015. Review of vapor condensation heat and mass transfer in the presence of non-condensable gas. Appl. Therm. Eng. 89, 469-484

Isenberg, J., Sideman, S., 1970. Direct contact heat transfer with change of phase: bubble condensation in immiscible liquid. Int. J. Heat Mass Tran. 13, 997-1011.

Jafari, R., Okutucu-Özyurt, T., 2016. 3D numerical modeling of boiling in a microchannel by arbitrary Lagrangian-Eulerian (ALE) method. Appl. Math. Comput. 272, 593-603.

Jeon, S.S., Kim, S.J., Park, G.C., 2011. Numerical study of condensing bubble in subcooled boiling flow using volume of fluid model. Chem. Eng. Sci. 66, 5899-5909.

Jia, H.W., Zhang, P., Fu, X., 2015. A numerical investigation of nucleate boiling at a constant surface temperature. Appl. Therm. Eng. 88, 248-257.

Jia, H.W., Xiao, X., Kang, Y.M., 2019. Investigation of a free rising bubble with mass transfer by an arbitrary Lagrangian-Eulerian method. Int. J. Heat Mass Tran. 137, 545-557

Kalman, H., 2003. Condensation of bubbles in miscible liquids. Int. J. Heat Mass Tran. 46, 3451-3463.

Kalman, H., Mori, Y.H., 2002. Experimental analysis of a single vapor bubble condensing in subcooled liquid. Chem. Eng. J. 85, 197-206.

Kalman, H., Ullmann, A., Letan, R., 1987. Visualization studies of a Freon-113 bubble condensing in water. J. Heat Tran. 109, 241-243.
Kalman, H., Ullmann, A., 1999. Experimental analysis of bubble shapes during condensation in miscible and immiscible liquids. J. Fluids Eng. 121, 496-502.
Kamei, S., Hirata, M., 1990. Condensing phenomena of a single vapor bubble into subcooled water. Exp. Heat Tran. 3, 173-182.
Kunkelmann, C., Stephan, P., 2009. CFD simulation of boiling flows using the volume-of-fluid method within OpenFOAM. Num. Heat Tran. Part A 56, 631-646.
Lee, K., Barrow, H., 1968. Transport process in flow around a sphere with particular reference to the transfer of mass. Int. J. Heat Mass Tran. 11, 1013-1026.
Lerner, Y., Kalman, H., Letan, R., 1987. Condensation of an accelerating-decelerating Bubble: experimental and phenomenological analysis. J. Heat Tran. 109, 509-517.
Magnini, M., 2012. CFD modeling of two-phase boiling flows in the slug flow regime with an interface capturing technique. University of Bologna Press.
Marek, R., Straub, J., 2001. The origin of thermocapillary convection in subcooled nucleate pool boiling. Int. J. Heat Mass Tran. 44, 619-632.
Marek, R., Straub, J., 2001. Analysis of the evaporation coefficient and the condensation coefficient of water, Int. J. Heat Mass Transfer 44, 39–53.
Oh, S., Revankar, S.T., 2006. Experimental and theoretical investigation of film condensation with noncondensable gas. Int. J. Heat Mass Tran. 49, 2523-2534.
Othmer, D.F., 1929. The condensation of steam. J. Ind. Eng. Chem. 21, 576-583.
Pan, L.M., Tan, Z.W., Chen, D.Q., Xue, L.C., 2012. Numerical investigation of vapor bubble condensation characteristics of subcooled flow boiling in vertical rectangular channel. Nucl. Eng. Des. 248, 126-136.
Plesset, M.S., Zwick, S.A., 1954. The growth of vapor bubbles in superheated liquids. J. Appl. Phys. 25, 493-500.
Poling, B.E., Prausnitz, J.M., Connell, J.P.O., 2004. The Properties of Gases and Liquids. The properties of gases and liquids. McGraw-Hill Companies Inc., New York, pp. 644-646.
Qu, X.H., Tian, M.C., 2016a. Acoustic and visual study on condensation of steam-air mixture jet plume in subcooled water. Chem. Eng. Sci. 144, 216-223.
Qu, X.H., Sui, H., Tian, M.C., 2016b. CFD simulation of steam-air jet condensation. Nucl. Eng. Des. 297, 44-53.
Revankar, S.T., Pollock, D., 2005. Laminar film condensation in a vertical tube in the presence of noncondensable gas. Appl. Math. Modelling 29, 341-359.
Sanjari, E., Hanarmand, M., Badihi, H., Ghaheri, A., 2013. An accurate generalized model for predict vapor pressure of refrigerants. Int. J. Refri. 30, 1327-1332.
Sato, Y., Ničeno, B., 2013. A sharp-interface phase change model for a mass-conservative interface tracking method. J. Comput. Phys. 249, 127-161.
Scriven, L.E., 1959. On the dynamics of phase growth. Chem. Eng. Sci. 10, 1-13.
Shang, D.Y., 2011. Theory of heat transfer with forced convection film flows. Springer Berlin Heidelberg.
Shen, B., Yamada, M., Hidaka, S., Liu, J., Shiomi, J., Amberg, G., Do-Quang, M., Takata, Y., 2017. Early onset of nucleate boiling on gas-covered biphilic surfaces. Sci. Rep. 7, 2036.
Slegers, L., Seban, R.A., 1970. Laminar film condensation of steam containing small concentrations of air. Int. J. Heat Mass Tran. 13, 1941-1947.
Tang, J., Yan, C., Sun, L., 2015. Effects of noncondensable gas and ultrasonic vibration on vapor bubble condensing and collapsing. Exp. Therm. Fluid Sci. 61, 210-220.
Tian, W., Ishiwatari, Y., Ikejiri, S.,Yamakawa, M., Oka, Y., 2010. Numerical computation of thermally controlled

steam bubble condensation using Moving Particle Semi-implicit (MPS) method. Annals. Nucl. Energy 37, 5-15.
Ullmann, A., Letan, R., 1989. Effect of noncondensibles on condensation and evaporation of bubbles. J. Heat Tran. 111, 1060-1067.
Zeng, Q., Cai, J., Yin, H., Yang, X., 2015. Numerical simulation of single bubble condensation in subcooled flow using OpenFOAM. Progr. Nucl. Energy 83, 336-346.
Zhang, P., Jia, H.W., 2016. Evolution of flow patterns and the associated heat and mass transfer characteristics during flow boiling in mini-/micro-channels. Chem. Eng. J. 306, 978-991.
Zheng, S., Eimann, F., Philipp, C., Fieback, T., Gross, U., 2018. Modeling of heat and mass transfer for dropwise condensation of moist air and the experimental validation. Int. J. Heat Mass Tran. 120, 879-894.